Part 3:
Physical ingredients of winds

https://doi.org/10.1017/S1743921322004598 Published online by Cambridge University Press

Winds of Stars and Exoplanets
Proceedings IAU Symposium No. 370, 2023
A. A. Vidotto, L. Fossati & J. S. Vink, eds.
doi:10.1017/S1743921322004598

The origin of planetary winds

Daria Kubyshkina

Space Research Institute, Austrian Academy of Sciences, Schmiedlstrasse 6, A-8042 Graz, Austria

Abstract. Atmospheric escape is a fundamental phenomenon shaping the structure and evolution of planetary atmospheres. Physics of planetary winds range from global processes such as tidal interactions with the host star, through large-scale hydrodynamic outflow, to essentially micro-physical kinetic effects, including Jeans-like escape and the interaction of planetary atmospheres with stellar winds and the own magnetic fields of planets. Each of these processes is expected to be most relevant for planets of different properties and at different stages in planetary and stellar evolution. Thus, it is expected that the hydrodynamic outflow guides the evolution of hydrogen-dominated atmospheres of planets having low masses (below that of Neptune) and/or close-in orbits, while the kinetic effects are most important for the long-term evolution of planets with secondary atmospheres, similar to the inner planets in the Solar System. Finally, each of these processes is affected by the interaction with stellar winds.

Keywords. hydrodynamics, atmospheric effects, planets and satellites: general

1. Introduction

Planetary winds, or atmospheric escape, represent the outflow of atmospheric material occurring on different space- and timescales. Depending on the age of the planet and the type of its atmosphere, planetary winds can be driven by a wide range of physical processes. Formally, these processes can be divided into thermal and non-thermal ones, where the former depends directly on the energy deposition in the atmosphere through heating, and the latter includes the processes related to microphysical interactions of the atmospheric species, to the interaction of the atmospheres with stellar winds, and to the effects related to the tidal or magnetic interaction with the host star. In Figure 1, I suggest a simplified classification of these processes.

The most classic form of thermal escape is the kinetic Jeans escape (e.g., Öpik 1963; Chamberlain 1963; Mihalas & Mihalas 1984), which assumes the atmospheres described by the Boltzmann distribution and considers the escape of the most energetic particles from the exobase, i.e., from the level where the atmosphere becomes collisionless. This approach implies that the fraction of particles with energies sufficient to overcome the escape velocity is small, and the whole atmosphere remains in a steady state without significant bulk motion. Such an assumption holds for the compact, terrestrial-like, secondary atmospheres or for the hydrogen-dominated atmospheres of Jupiter-like planets in absence of the significant energy input from an external source. With increasing energy input, the thermal energy of the atmospheric gas grows. At some point, the bulk energy of the atmospheric material overcomes the gravitational well of the planet and forms a continuous bulk outflow (e.g., Watson et al. 1981). This case is considered by the hydrodynamic approach, assuming collisional, fluid-like atmospheres.

In the case of hydrodynamic escape, the outflow can be supported by different energy/heating sources. The most common one is the heating by the high-energy stellar

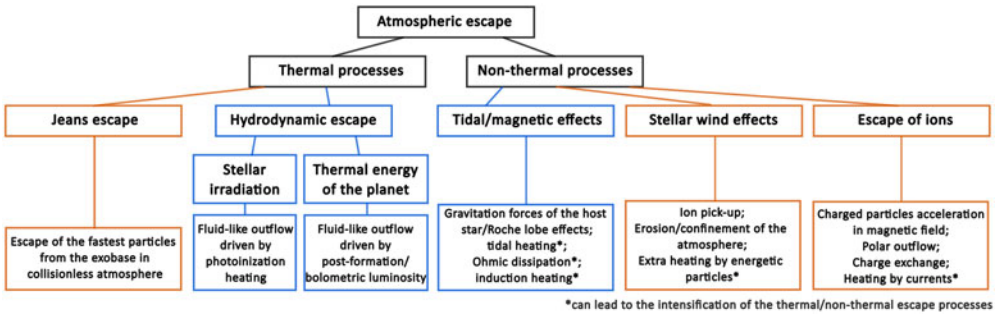

Figure 1. A simplified scheme reflecting the most common types of atmospheric escape, i.e., the mechanisms driving planetary winds. The color of the boxes highlights kinetic processes mainly relevant in the case of secondary atmospheres (orange) and hydrodynamic/global processes that have a major impact on voluminous hydrogen-dominated atmospheres (blue).

irradiation (X-ray + extreme ultraviolet, XUV) absorbed deep in the upper atmosphere. However, the hydrodynamic planetary wind can be also driven by the heat deposited in the planetary core/lower atmosphere, such as the post-formation cooling luminosity of a planet or bolometric heating from the host star.

Non-thermal escape processes, in turn, can be split into three groups: the tidal/magnetic interaction with the host star, interaction with stellar winds, and the ion escape processes at magnetized and non-magnetized planets. The tidal forces of the host star are relevant for the escaping atmospheres of planets in close-in orbits, and their influence can be twofold. First, stellar gravity forces can interact with atmospheric material directly, decreasing the energy needed for the atmospheric particles to leave the gravitation well of the planet. In extreme cases of very small orbital distances, the Roche lobe (the obstacle within which the atmosphere is gravitationally bound to the planet) comes close to the planetary photosphere resulting in the catastrophic Roche lobe overflow (Koskinen et al. 2022). Second, the tidal heating in the lower levels of the atmosphere (e.g., Bodenheimer et al. 2001; Arras & Socrates 2010) can lead to planetary inflation and to the intensification of the thermal escape processes due to the increase in the energy budget of the atmosphere. A similar effect can be caused by the magnetic interaction between the star and a close-in planet, through the induction of currents deep in the atmosphere (e.g., Batygin & Stevenson 2010; Wu & Lithwick 2013; Ginzburg & Sari 2016; Kislyakova et al. 2018). For further detail on these processes, I point the reader to the recent review by Fortney et al. (2021).

Stellar winds represent the hot coronal material (low-density plasma) accelerated to high velocities and carrying stellar magnetic field (see, e.g., Vidotto et al. 2015). Their interaction with planetary atmospheres depends strongly on the presence of planetary magnetic field (see, e.g., Cohen et al. 2022), parameters of the planet (e.g., Carolan et al. 2020) and age of the system (e.g., Kubyshkina et al. 2022). Along with the erosion of planetary atmospheres, extra heating of atmospheres by stellar wind energetic particles, and ion pick-up (drag of ions from the exosphere due to the interaction with the electromagnetic field of the wind), increasing the atmospheric mass loss, stellar winds can confine planetary atmospheres leading to the reduction of the escape if the pressure balance is reached close to the planet (e.g., Christie et al. 2016; Vidotto & Cleary 2020; Carolan et al. 2020, 2021).

The wide range of non-thermal escape processes, including ion pick-up by the stellar wind, relates specifically to the escape of the ionized species, and depends, therefore, on the presence, strength, and configuration of the planetary magnetic field. This includes precipitation of energetic particles/ions from the upper atmosphere, interaction with

https://doi.org/10.1017/S1743921322004598 Published online by Cambridge University Press

energized particles from stellar winds or the ionosphere, the processes controlled by the magnetic field of the planet (as polar outflow and acceleration of the particles on closed magnetic lines), and processes driven by photochemistry. All these processes strongly depend on the specific content of planetary atmospheres.

Besides the division into thermal and non-thermal processes, the processes described above can be split into kinetic (indicated by orange boxes in Figure 1) and large-scale hydrodynamic/tidal effects (blue boxes). In general, all of these processes can occur simultaneously and can take place at any planet. Their relative input in driving planetary wind, however, differs depending on the age of the planet (and its host star) and the type of atmosphere. Thus, the hydrodynamic escape (predicting the largest atmospheric mass loss rates among the processes discussed here) plays a major role for primary hydrogen-dominated atmospheres. It drives, therefore, the winds of young planets and of close-in Neptune-like/Jupiter-like planets. The kinetic escape processes, in turn, are relevant for compact secondary (terrestrial-like) atmospheres.

In the following sections, I consider the mechanisms outlined above in more detail. I focus predominantly on the hydrodynamic outflow, and for more detail on the kinetic escape processes, I point the reader to the recent and detailed review by Gronoff et al. (2020). Here, I start with describing the Jeans escape in section 2.1 and give a brief overview of the ion escape from non-magnetized and magnetized planets in sections 2.2 and 2.3. In section 3 I describe the typical approach to the hydrodynamic outflow and discuss in more detail the XUV-driven escape (section 3.1), the hydrodynamic escape driven by the own thermal energy of a planet (section 3.2), and the tidal effects in this context (section 3.3). I describe the influence of the hydrodynamic escape across the wide parameter range in section 3.4 and discuss the influence of magnetic fields on these escape processes in section 4. I summarize my conclusions in Section 5.

2. Kinetic escape processes

In this chapter, I briefly discuss the variety of microphysical/kinetic processes driving atmospheric escape. Though the typical atmospheric escape rates associated with such processes are at least an order of magnitude below those of the hydrodynamic escape, the kinetic processes are crucial for the evolution of planets and their atmospheres. Specifically, the timing and relative input of different thermal and non-thermal processes control the fractionation of chemical elements and their isotopes, and therefore essentially control the atmospheric content. For more information, I point the reader to the recent review on the fractionation of noble gases and other heavy elements including a description of all atmospheric fractionation processes by Lammer et al. (2020b).

2.1. *Jeans escape*

Jeans escape represents the most classic form of thermal escape considering the kinetic escape of most energetic particles in the atmosphere. To evaluate it in the most accurate way, one has to solve the Boltzmann equation (see, e.g., Volkov et al. 2011). However, given the computational costs of such a method, a range of simplifications are commonly applied. In the most common approach, the atmosphere is considered Maxwellian (Mihalas & Mihalas 1984)

$$f(\vec{x},\vec{v}) = n_{\rm i}\left(\frac{1}{\pi u_{\rm th,i}^2}\right)^{3/2} \exp\left(-\frac{v^2}{u_{\rm th,i}^2}\right), \tag{2.1}$$

where $n_{\rm i}$ is the numerical density, and $u_{\rm th,i} = \sqrt{\frac{2k_{\rm b}T}{m_{\rm i}}}$ is a thermal velocity of i-th atmospheric species with the mass $m_{\rm i}$; atmospheric temperature T is assumed to be constant.

https://doi.org/10.1017/S1743921322004598 Published online by Cambridge University Press

The most energetic particles in this distribution, with velocities $v > v_{\rm esc} = \sqrt{\frac{2GM_{\rm pl}}{r}}$ at the exobase (where $M_{\rm pl}$ is the planetary mass and r is the radial distance from the planet center), escape. With such an approach, the flux of escaping particles depends on the relation between the escape velocity and the thermal speed

$$\Phi = n_{\rm i} \left(\frac{u_{\rm th,i}^2}{4\pi} \right)^{1/2} (1 + \lambda_{\rm exo}) \exp(-\lambda_{\rm exo}) \,. \tag{2.2}$$

Parameter $\lambda_{\rm exo} = \frac{v_{\rm esc}^2}{u_{\rm th,i}^2} = \frac{GM_{\rm pl} m_{\rm i}}{k_{\rm b} T_{\rm exo} r_{\rm exo}}$ (Jeans parameter) represents, in a more general sense, the relation of the gravitational energy of the planet to the thermal energy deposited in its atmosphere calculated at exobase. Besides controlling the flux 2.2, or the atmospheric mass loss rate in terms of thermal atmospheric escape, this relation is used to distinguish between the Jeans and the hydrodynamic regimes. As discussed in the introduction, with increasing thermal energy the atmospheric outflow changes qualitatively – the mean energy of the particles becomes high enough to overcome the gravity of the planet itself and the binding due to the collisions between the atmospheric particles, allowing for the planetary wind to engage deep below the exobase level. The border value of $\lambda_{\rm exo}$ was estimated 1-3 upon different assumptions (Hunten 1982; Volkov et al. 2011; Erkaev et al. 2015).

Differently to the hydrodynamic escape, where the dense outflow of light elements (such as hydrogen and helium) can drag away the heavier elements (e.g., Zahnle & Kasting 1986; Hunten et al. 1987; Pepin 1991; Odert et al. 2018; Lammer et al. 2020a; Erkaev et al. 2022), in "collisionless" Jeans escape the escape of different species occurs almost independently. Therefore, in quiet conditions, Jeans escape can describe the escape of lighter particles through the stable heavy-element atmospheres, as, e.g., escape of hydrogen and helium from the present-day Earth, Venus, and Mars (Shizgal & Blackmore 1986; Chamberlain 1969; Hunten 1973). This makes Jeans escape particularly important for the fractionation of light elements in planetary atmospheres.

Summarizing the above, the Jeans escape is most relevant for the atmospheric escape from planets exposed to the thermal escape but remaining under moderate conditions, i.e., with energy input that is non-negligible but also not too large (as in the case of close-in exoplanets or young host stars). The atmospheres of such planets are expected to remain stable. Therefore, Jeans escape typically defines the outflow from compact secondary atmospheres of terrestrial-like planets in evolved (ages of a few Gyr) planetary systems or from cool gas giants with hydrogen-dominated atmospheres close to the hydrostatic equilibrium. In the latter case, and also for $\lambda_{\rm exo}$ close to the border values, the atmospheric mass loss rates given by this approach become comparable to slow hydrodynamic outflow.

The formulation of the Jeans escape presented here has a range of limitations. The real distribution of the atmospheric particles is not quite Maxwellian, especially in the case of strong Jeans escape, and the atmosphere is not isothermal; escape also does not occur only from exobase. The range of corrections exists to account for these facts (see Gronoff et al. 2020, and the references therein) but in the most general case one has to solve the Boltzmann equation to get the most accurate estimate. Also, if one aims at using equation 2.2 as an analytical approximation, one needs to know the position and parameters of the atmosphere at the exobase. In the case of exoplanets, these parameters are typically unknown, while they can vary significantly through the evolution and across planetary parameter space (e.g., Lammer et al. 2008).

https://doi.org/10.1017/S1743921322004598 Published online by Cambridge University Press

2.2. *Ion escape from non-magnetized planets*

The relevance of non-thermal processes in general, as well as the relevance of every specific mechanism, varies between different planets and depends on its basic parameters, such as mass and orbital separation, atmospheric composition, and the age/activity level of the host star. For highly irradiated planets, the atmospheric mass loss rates of non-thermal escape processes described here and in the next section are typically about an order of magnitude lower than thermal escape. However, they remain significant for terrestrial planets, and can even dominate in quiet conditions, as they are expected to be progressively more important with decreasing stellar irradiation and increasing age (e.g., Vidal-Madjar 1978; Shizgal & Lindenfeld 1982). Thus, in the present-day solar system, the dominant escape source is represented by various ion escape processes considered in this section.

The atmospheric species can be ionized through a few channels, of which the dominant one is photoionization by stellar irradiation. Additionally, ions can be produced by collisions with the atmospheric electrons or the energetic particles of the stellar wind. Thus, a large fraction of the species in the upper layers of the planetary atmosphere (exosphere) are represented by ions of different atoms/molecules. In the case of non-magnetized planets, these ions can be removed from the exosphere through ion pick-up (see, e.g., Kislyakova et al. 2013): the ionized particles interact with the magnetic field frozen in the stellar wind plasma and can be dragged away. This process is effective both on terrestrial-like planets and the gas giants; the associated atmospheric mass loss rates remain, however, several times smaller than those of thermal Jeans escape for different planetary types.

Further on, photochemical reactions and collisions with stellar wind particles can also lead to additional heating (and thus, larger thermal escape) and the production of energetic neutral atoms (ENA) with energies sufficient to escape the gravitation well of the planet (e.g., Shizgal & Arkos 1996; Shematovich et al. 1994; Lee et al. 2015) and sputtering of atmospheric species (e.g., Johnson 1994; Johnson et al. 2008).

Among the exothermic photochemical reactions, except the photoionization which will be discussed in more detail in the context of hydrodynamic escape in section 3, the most relevant appear the photodissociation and ion recombination processes. These processes are specifically relevant for the escape of heavy ions, and in the present-day solar system dominate the escape of oxygen, nitrogen, and carbon species (O^+, NO^+, CO^+, CO_2^+) from Earth and Mars (see Gronoff et al. 2020, and references therein).

In terms of fractionation of elemental and isotopic abundances, non-thermal escape processes, similar to Jeans escape, are most relevant for the evolution of secondary atmospheres, after the removal of primordial hydrogen-dominated envelopes by hydrodynamic winds. Differently from Jeans escape, the non-thermal processes are capable of the fast removal of heavy ions, though the former can yet be more effective on longer timescales (e.g., Kulikov et al. 2007; Lammer et al. 2020b).

The study of non-thermal escape processes from exoplanets is complicated by the fact, that the overall picture is strongly dependent on the specific content of the atmosphere, which is, in general, unknown. Therefore, in the ideal case, such studies require testing the stability of the assumed atmosphere in the context of the long-term evolution accounting for the activity history of the host star.

2.3. *Interaction of ions with magnetic fields*

With the inclusion of magnetic fields, the behavior of neutral and ionized species becomes rather different. While the neutrals "do not notice" the magnetic field and escape in a regular way (e.g., through Jeans escape), the motion of the charged particles

https://doi.org/10.1017/S1743921322004598 Published online by Cambridge University Press

is bound in a presence of the magnetic field and spiraled/circularized along the field lines. Thus, in the regions where magnetic lines are closed, the charged particles are getting trapped.Instead, in the regions of open magnetic field lines (as polar cusps and reconnection regions), the escape of ionized species intensifies. The escape of plasma from the ionosphere through the polar cusps (so-called polar wind/polar outflow) can reach the mass loss rates comparable to hydrodynamic escape (see, e.g., Carolan et al. 2021).

Further on, in the case of a dipole-like field charged particles can be accelerated in the "magnetic mirror", making oscillatory motion along the line with magnetic field strength increasing towards both ends approaching the planet until they reach the energy sufficient to escape. The charged particles can escape from the line if their pitch angle (between their velocity vector and the magnetic field direction) is sufficiently small. Otherwise, the escape occurs through charge exchange – the collision of an energized ion with a neutral atmospheric atom leading to the production of the energized neutral atom, that can escape, e.g., through Jeans escape, and a regular ion

$$\mathrm{M}^{*+} + M \rightarrow M^{*} + M^{+} \,. \tag{2.3}$$

The same process can be an effective source of escape also through the collisions of neutrals with energetic ions from the ionosphere and the stellar wind.

Finally, in presence of a magnetic field, numerous current systems appear at the magnetopause and across the ionosphere, which can provide additional heating intensifying the thermal atmospheric escape.

3. Hydrodynamic escape

In contrast to the kinetic Jeans escape discussed in Section 2.1, in the hydrodynamic approach an atmosphere is treated as a collisional, fluid-like medium. Gross (1972) have demonstrated that in case of substantial (hence, dense) hydrogen-dominated atmospheres the temperatures at the exobase can rise to the values order of 10000 K and the values of λ_{exo} drop below 1. In this case, the total internal (thermal) energy of the atmospheric gas exceeds the energy of the gravitation well binding the atmospheric material to the planet, and the atmospheric escape represents a bulk outflow rather than the loss of individual particles from the exobase.

Already decades ago, this approach was used to study the early evolution of Earth and Venus (see, e.g., Dayhoff et al. 1967; Sekiya et al. 1980; Watson et al. 1981), and later on it was generalized on the hydrogen-dominated atmospheres of extrasolar planets, specifically close-in Jupiter-like and sub-Neptune-like planets (see, e.g., Lammer et al. 2003; Lecavelier des Etangs et al. 2004; Yelle 2004; Cecchi-Pestellini et al. 2009; Owen & Jackson 2012; Erkaev et al. 2016; Kubyshkina et al. 2018; Caldiroli et al. 2021). For substantial hydrogen-dominated atmospheres of close-in planets, the hydrodynamic escape represents the major source of the atmospheric mass loss, overcoming by an order of magnitude kinetic and non-thermal escape processes discussed in Section 2. Therefore, it is believed to be the main driving mechanism of the atmospheric evolution (e.g., Murray-Clay et al. 2009; Lopez et al. 2012; Chen & Rogers 2016; Kubyshkina et al. 2019, 2020) and therefore to play a major role in shaping the population of low to intermediate mass exoplanets as it is known to date (e.g., Fulton et al. 2017; Fulton & Petigura 2018; Owen & Wu 2017; Gupta & Schlichting 2019; Mordasini 2020).

In general, the hydrodynamic outflow from a planet is described by a set of fluid dynamics equations, which can be written in a 1D form as

$$\frac{\partial \rho}{\partial t} + \frac{\partial (\rho v r^2)}{r^2 \partial r} = S \,, \tag{3.1}$$

$$\frac{\partial \rho v}{\partial t} + \frac{\partial [r^2 (\rho v^2 + P)]}{r^2 \partial r} = -\frac{\partial U}{\partial r} + \frac{2P}{r} \,, \tag{3.2}$$

https://doi.org/10.1017/S1743921322004598 Published online by Cambridge University Press

$$\frac{\partial E}{\partial t} + \frac{\partial[vr^2(E+P)]}{r^2\partial r} = Q + \frac{\partial}{r^2\partial r}(r^2\chi\frac{\partial T}{\partial r}) - \frac{\partial(\rho U)}{r^2\partial r}\,. \tag{3.3}$$

These three equations describe the mass, momentum, and energy conservation, and the variables are the radial distance from the planet along the substellar line (r), density (ρ), temperature (T), and bulk velocity (v) of the atmosphere, thermal pressure (P), the sum of the kinetic and thermal energies (E), and the gravitational potential U, which can represent the gravitational potential of the central body (planet) or account also for the gravitational forces of the host star (Erkaev et al. 2007). The source term S on the right-hand of equation 3.1 is typically taken as 0, reflecting the assumption that there are no leaks or replenishment of the atmospheric material. Finally, the second term in Equation 3.3 accounts for the thermal conductivity of the neutral gas ($\chi = 4.45 \times 10^4(\frac{T[\mathrm{K}]}{1000})^{0.7}\,\mathrm{erg\,cm^{-1}\,s^{-1}}$).

The term Q in Equation 3.3 represents the sum of all heating and cooling processes accounted for in the specific model. The number and the type of the specific cooling/heating processes thus depend on the chosen approach and the specific composition of the hydrogen-dominated atmosphere. However, the main heating source is normally the photoionization of the atmospheric species (in primary atmospheres, predominantly, ionization of hydrogen by the XUV radiation of the host star)

$$\mathrm{M} + h\nu \rightarrow \mathrm{M}^+ + e^*\,. \tag{3.4}$$

In this reaction, the stellar photon of a certain energy ($h\nu$) heats the atmospheric particle M. If the energy of a photon exceeds the ionization threshold of the particle, it leads to the production of an ionized particle and a free electron, that carries away the excess energy (given by the difference between the energy of the photon and the ionization energy). This excess energy can be further lost in the collisions (leading to the heating of the atmosphere) or spent in other, endothermic, reactions, such as recombination or secondary ionization of atmospheric species. Therefore, to accurately define which fraction of the absorbed photon energy is spent on heating, one has to account for all relevant reactions and also for all energy levels of the atmospheric species, as the electron tore away in reaction 3.4 must not be the one with the minimal ionization energy in the general case. The resulting heating efficiency, i.e., the relation of the energy spent on heating to the total absorbed energy, varies with altitude and the wavelength (energy) of the incident radiation, and also depends on the type of a planet (Dalgarno et al. 1999; Yelle 2004; Shematovich et al. 2014; Salz et al. 2015, 2016a,b). Given the application complexity and the numerical costs of such an approach, the real heating efficiency is often reduced to a coefficient η, which is further set to a constant value (as, e.g., in Owen & Jackson 2012; Erkaev et al. 2016; Kubyshkina et al. 2018) or has an analytical dependence on the photon wavelength (as in Murray-Clay et al. 2009; Allan & Vidotto 2019; Kubyshkina et al. 2022). In this case, the volume heating rate of species "i" by the stellar flux of wavelength ν can be written as

$$H_{ion} = \frac{\eta\sigma_{\nu,i}n_{\mathrm{i}}}{2}\int_0^{\frac{\pi}{2}+\arccos(1/r)} I_{\nu,i}(r,\theta)\sin\theta d\theta\,, \tag{3.5}$$

where n_{i} is the numeric density of species "i", $\sigma_{\nu,i}$ is the wavelength-dependent absorption cross-section, and $I_{\nu,i}(r,\theta)$ describes the spatial variations of the stellar irradiation due to the atmospheric absorption in spherical coordinates.

Other heating and cooling sources are given by other exothermic and endothermic reactions, such as, e.g., collisional excitation of hydrogen (Lyα-cooling)

$$\mathrm{H} + e^* \rightarrow H^* + e\,. \tag{3.6}$$

https://doi.org/10.1017/S1743921322004598 Published online by Cambridge University Press

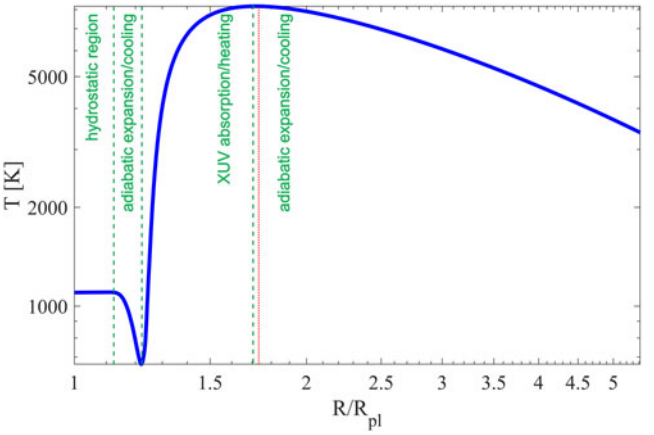

Figure 2. A typical temperature profile of the hot, strongly irradiated sub-Saturn. The mass of the planet is 45.1 $M_{\oplus}$and the radius is 6.0 $R_{\oplus}$. It is located at 0.04 AU from its 0.8 $M_{\odot}$host star (which corresponds to the equilibrium temperature of 1100 K), and receives the XUV flux of $\sim$54000 $erg/s/cm^2$. The mass loss rate estimated in hydrodynamic simulation is 6.8×10^{10} g/s.

The corresponding cooling/heating rates are given by the product of the numerical densities of participating species and the specific reaction rates

$$C_{Ly\alpha} = 7.5 \times 10^{-19} n_e n_H exp\left(\frac{118348\text{K}}{T}\right). \quad (3.7)$$

To account for these processes (which typically include photodissociation, recombination, collisional ionization, etc.), in addition to the Equations 3.1–3.3 one has to solve the system of equations describing chemical equilibrium. It consists of equations in a form of Equation 3.1 on numerical densities for each individual species included in the specific model, where the source terms represent the sink/replenishment of the species according to chemical reactions.

3.1. *XUV-driven outflow*

The most common and widely studied type of the hydrodynamic escape is an XUV-driven escape, which considers the photoionization heating as the main driving mechanism of the hydrodynamic wind (e.g., Watson et al. 1981; Yelle 2004; Lecavelier des Etangs et al. 2004; Murray-Clay et al. 2009; Owen & Jackson 2012; Shematovich et al. 2014; Salz et al. 2016a; Erkaev et al. 2016; Kubyshkina et al. 2018; Caldiroli et al. 2021). In this approach, the deep layers of otherwise hydrostatic atmosphere are heated up by the stellar irradiation leading to the adiabatic expansion and settling of the transonic planetary wind. In Figure 2, I show a typical temperature profile for the upper atmosphere of the planet experiencing XUV-driven atmospheric escape. The planet is a 45.1 $M_{\oplus}$ and 6.0 $R_{\oplus}$ sub-Saturn orbiting at 0.04 AU around 0.8 $M_{\odot}$ star and receiving the XUV flux of $\sim$54000 $erg/s/cm^2$. According to the hydrodynamic model, it experiences an atmospheric mass loss of 6.8×10^{10} g/s. Here and later in this section, we employ the hydrodynamic model by Kubyshkina et al. (2018) for the examples, unless stated otherwise. It is a 1D model assuming a pure hydrogen atmosphere and accounting for the effects of dissociation, recombination of ions and of the atomic hydrogen to H_2, collisional ionization, Lyα-cooling, and H_3^+-cooling. The stellar irradiation is treated in two bands of 5 nm (X-ray) and 62 nm (EUV), and the constant heating efficiency of 0.15 is assumed in both cases.

https://doi.org/10.1017/S1743921322004598 Published online by Cambridge University Press

In Figure 2, one can see a few distinct regions. The lower boundary ($R = R_{pl}$) of the simulation domain is the observable radius of the planet, i.e., the photosphere. The lowermost region (up to $R \simeq 1.1 R_{pl}$) is gravitationally well bound to the planet and remains hydrostatic, which can be seen by the constant temperature. Higher up, the gravitation force of the planet decreases, and the atmosphere starts to expand adiabatically, and, therefore, to cool (1.1–1.2 R_{pl}). The XUV irradiation of the specific wavelength penetrates the atmosphere layers that are optically thin for this layer and is absorbed at the specific height where the optical depth τ becomes 1. This height lies deeper in the atmosphere for more energetic (short-wavelength) radiation, and higher for the less-energetic part of the spectra. Therefore, the ionizing radiation (energetic enough to tear away the electron from the hydrogen atom) heats the atmosphere in the narrow region somewhat above the photosphere of the planet (1.2–1.7 R_{pl} in Figure 2). Then at some point, the heating is overtaken by adiabatic cooling, and the atmosphere expands up to and beyond the Roche lobe, which is a natural upper boundary of the simulation domain where the gravitation forces of the planet and its host star equilibrate. Above this point, the atmosphere is no more gravitationally bound to the planet.

In terms of other parameters, the outflow represents the upward accelerating wind with density gradually decreasing and ion fraction gradually increasing with radial distance.

The planet discussed above represents the most classic case of the XUV-driven planetary wind. Such a picture is typical for the high gravity planets with well-bound atmospheres. In a more general case, some regions shown in Figure 2 can degenerate. For example, the lowermost hydrostatic region can be absent in the case of the planet with lower gravity or higher thermal energy (see the next section 3.2 for more detail); the inner region of adiabatic cooling (and thus the temperature minimum) can degenerate for massive planets with a very steep density gradient in the inner region; finally, if the Roche lobe is located close to the planet, which is typical for low-mass planets orbiting close to their host stars, the upper region of the adiabatic expansion/cooling can be absent and the heating occurs in the uppermost layers of the upper atmosphere. In the next sections, I consider some extreme cases.

3.2. *Hydrodynamic outflow driven by the own thermal energy of a planet*

Until recently, the XUV irradiation was considered to be the major, and the only relevant, source of energy fuelling the hydrodynamic outflow. Thus, e.g., Sekiya et al. (1980) considers as an additional source of the heating a release of the gravitational energy due to the planetesimal accretion for Earth but concludes that this source is minor in comparison to the stellar high-energy radiation. However, if considering the whole diversity of exoplanets at different stages of evolution, the own thermal energy of the planet can play a crucial role in powering the planetary wind. To account for this type of atmospheric escape, Ginzburg et al. (2016b, 2018) introduced the term "core-powered mass loss" and suggested the post-formation luminosity as the energy source. Later, Gupta & Schlichting (2019) generalized this idea for the bolometric heating from the host star. Given that the post-formation luminosity and the inflation degree of a planet decline with time, the relative input of this atmospheric escape mechanism in comparison to the XUV-driven escape (that occurs on Gyr timescale, see, e.g., King & Wheatley 2021) is expected to be largest for young planets.

For the own thermal energy of the planet to be the major driver of the planetary wind, this energy should dominate the gravitational energy binding the planetary atmosphere. Thus, this type of planetary wind is typical for low-gravity, hot, and/or highly inflated planets. For a prime example, I consider in Figure 3 a hot super-puff type planet of the low mass (2.1 $M_\oplus$) and a radius of 3.0 $R_\oplus$ orbiting at 0.04 AU around 0.8 $M_\odot$ K-type

https://doi.org/10.1017/S1743921322004598 Published online by Cambridge University Press

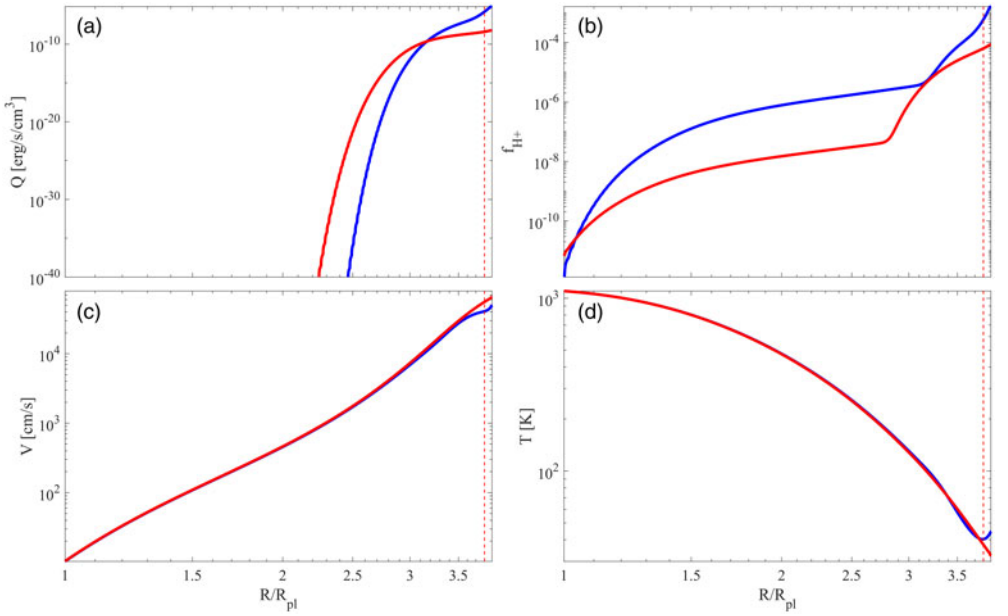

Figure 3. Volume heating rate (a), ion fraction (b), bulk velocity (c), and temperature (d) of the atmosphere of the low gravity planet against radial distance. The red and the blue lines correspond to low ($F_{\rm XUV} = 140$ erg/s/cm^2) and high ($F_{\rm XUV} = 56000$ erg/s/cm^2) XUV irradiation levels, respectively. The mass of the planet is 2.1 $M_\oplus$ and the radius is 3.0 $R_\oplus$. It is located at 0.04 AU from its 0.8 $M_\odot$ host star (which corresponds to the equilibrium temperature of 1100 K). The mass loss rate estimated in hydrodynamic simulations is $\sim 3.5 \times 10^{14}$ g/s for both cases.

star. These parameters correspond to a low density of about 0.4 g/cm^3, suggesting that the planet hosts a large and massive hydrogen-dominated atmosphere (in the case of an evolved planet) or is inflated due to the heat deposited in the planetary core/lower atmosphere (in the case of a young planet). In principle, the hydrodynamic model does not distinguish between the two cases, as the lower boundary of the simulation domain lies at the photosphere. The condition of the lower atmosphere is, therefore, set by the atmospheric parameters fixed at the lower boundary; in the example considered here I adopted the photosphere pressure of ∼0.13 bar and the photosphere temperature equal to the equilibrium temperature assuming zero albedos (1100 K) based on the results of the lower atmosphere modeling for the first case (large atmospheric mass fraction Cubillos et al. 2017).

Due to the low gravity of the planet considered in Figure 3, the atmosphere is less gravitationally bound and the density gradient is less steep than at the planets considered in section 3.1, where most of the atmospheric material is concentrated in the inner region. It leads to a dense and relatively slow outflow. The atmospheric density remains high up to the Roche lobe, preventing stellar XUV from penetrating into the deep layers and thus, from effectively heating the atmosphere. In Figure 3, I consider two very different levels of XUV flux exposed at the planet: very low (accounting for the position of the planet) one of 140 erg/s/cm^2 (red lines) and the high one of 56000 erg/s/cm^2 (blue lines). One can see, that despite the very different levels of irradiation, the velocity and temperature profiles (bottom panels of Figure 3) are nearly identical in the two cases. The same holds also for the density profiles not shown here. This is due to the volume heating rate and the ion fraction remaining very low throughout the atmosphere (top panels of Figure 3), and the XUV heating being therefore inefficient, as discussed above.

https://doi.org/10.1017/S1743921322004598 Published online by Cambridge University Press

The inefficiency of the XUV heating does not mean, however, that the planetary wind is absent in this case. Instead, it is driven by the pressure gradient between the lower and the upper atmosphere, and the atmospheric mass loss rates in both considered cases are exceptionally high – $\sim 3.5 \times 10^{14}$ g/s. This suggests, that at this planet (with the wind purely driven by its own thermal energy) the atmosphere is not stable and will escape within a short time order of megayear. Therefore, one would not expect such a planet to be present among the evolved population and such a mechanism to be important out of the initial stages of planetary evolution. However, for less extreme cases, the own thermal energy of the planet can yet be relevant along with the stellar XUV heating and contribute to driving planetary winds on longer timescales.

3.3. *Tidal effects*

Besides the energy (heating) sources considered in sections 3.1 and 3.2, the important role in controlling planetary winds can be played by the tidal interactions with the host star, specifically for close-in planets. As I already mentioned in the Introduction, the interaction of close-in planets with their host stars, magnetic or tidal, can lead to additional heating in the lower layers of the atmospheres and therefore intensify the thermal escape processes, specifically those described in sections 2.1 and 3.2, and it can also affect the ion escape processes. Here, I will discuss a more direct implication of tidal forces onto the atmospheric material relevant in terms of hydrodynamic outflow.

Accounting for the tidal effects, the gravitation potential along the substellar line can be written as (Erkaev et al. 2007)

$$\mathbf{U} = \mathbf{U_0}\left[-\frac{\mathbf{1}}{\zeta} - \frac{\mathbf{1}}{\mu(\xi-\zeta)} - \frac{\mathbf{1}+\mu}{\mathbf{2}\mu\boldsymbol{\xi}^{\mathbf{3}}}\left(\xi\frac{\mathbf{1}}{\mathbf{1}+\mu} - \zeta\right)^{\mathbf{2}}\right]. \tag{3.8}$$

In Equation (3.8), $U_0 = GM_{\rm pl}/R_{\rm pl}$, $\mu = M_{\rm pl}/M_*$, $\xi = a/R_{\rm pl}$, and $\zeta = r/R_{\rm pl}$ (where a is the orbital separation and r is the radial distance from the planet). The second term in the square brackets accounts for the effects of the stellar gravitation forces, and it is easy to see that their role increases with increasing distance from the planet along the substellar line, and, more generally, with decreasing orbital separation and decreasing $M_{\rm pl}/M_*$ ratio. The latter changes from the values order of 10^{-2} in the case of the Jupiter-like planets orbiting M-dwarfs to $\sim 10^{-6}$ for Earth-like planets orbiting G or F-type stars. The term ξ, in turn, reflects the fact that for two identical planets (the same mass, radius, and equilibrium temperature) the tidal effects are larger around the lower-mass host star, as the same temperatures are reached at shorter orbits compared to heavier stars.

For an extreme example, in Figure 4 I compare the atmospheric models for the hot dense Neptune-mass planet orbiting stars of $0.8\,M_\odot$ (at ~ 0.02 AU, blue lines) and $0.4\,M_\odot$ (at ~ 0.004 AU, red lines). The most evident difference between the two cases is the position of the Roche lobe: about $6\,R_{\rm pl}$ in the first case, and only about $1.5\,R_{\rm pl}$ in the second one. Thus, in the first case (more massive host star), the atmospheric outflow represents a typical case of the XUV-driven escape (see the temperature profile in panel (c) of Figure 4), as expected for such a high-gravity planet. The mass loss rate estimated in this case is $\sim 2.0 \times 10^8$ g/s, which is slightly lower than the value predicted for the given XUV flux (391 erg/s/cm^2) by energy-limited approximation adopting the form from Erkaev et al. (2007). It is expected for this type of planet and highlights that the atmospheric outflow is purely XUV-driven, without significant input from the own thermal energy of the planet.

For the planets orbiting $0.4\,M_\odot$star, the outflow looks completely different. As the Roche lobe is located so close to the photosphere, the gravitation forces of the planet are only effective within $\sim 1\,R_\oplus$ distance from the photosphere of the planet. Moreover,

https://doi.org/10.1017/S1743921322004598 Published online by Cambridge University Press

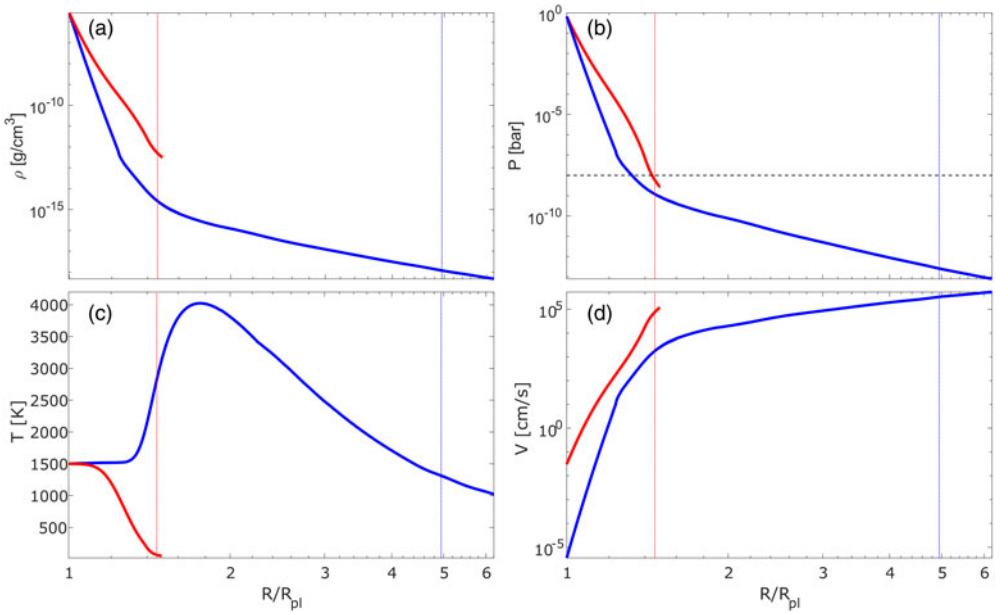

Figure 4. Density (a), pressure (b), temperature (c), and bulk velocity (d) profiles of the two planets of equivalent radius (2.0 $R_\oplus$), mass (16.2 $M_\oplus$), and equilibrium temperature (1500 K), and under similar levels of XUV irradiation (about 400 erg/s/cm^2), but orbiting different stars (which means, that the given T_{eq} is achieved at different orbital distances). The blue solid lines correspond to the planet orbiting 0.8 $M_\odot$star at 0.0194 AU, and the red solid lines to the planet orbiting 0.4 $M_\odot$star at 0.0037 AU. The blue/red dashed vertical lines denote the positions of the sonic points in the respective simulations. The horizontal black dashed line in panel b denotes the 10 nbar level (Roche lobe overflow limit; Koskinen et al. 2022).

comparing the input from the planet into gravitation potential (the first term in the square brackets in Equation 3.8) to the stellar input (the second term in the square brackets), one can see that the stellar gravitational forces remain crucial even within this region. As a result of the shortness of the Roche radius and the impact of the stellar tidal forces, the atmosphere remains very dense up to the Roche lobe (see panel (a) of Figure 4) and the outflow occurs in a manner similar to the case described in section 3.2. However, as the own thermal energy of the planet is relatively small in this case (about 1.5 orders of magnitude below the gravitational one), the outflow is mainly controlled by the tidal forces. The atmospheric mass loss rate estimated in this simulation is $\sim 1.7 \times 10^{12}$ g/s, which is about 3 orders of magnitude above the one given by the energy-limited equation for the XUV flux of 496 erg/s/cm^2. As one can see from panel (b) of Figure 4, the pressure at the upper boundary is consistent with the lower limit predicted for the Roche lobe overflow by Koskinen et al. (2022) (10-100 nbar).

As in the case of the planetary wind driven by the own thermal energy of the planet considered in the previous section, the example presented here is quite extreme (the model planet may even not be physical). This was done to surely isolate the effect of the tidal forces. However, also for more moderate planets, tidal effects can have a significant effect. I discuss it in more detail in the next section.

3.4. *Atmospheric mass loss rates across parameter space*

In this section, I give a brief summary of the mechanisms driving the hydrodynamic planetary winds discussed in sections 3.1–3.3 and consider their influence across the

https://doi.org/10.1017/S1743921322004598 Published online by Cambridge University Press

parameter space. To this end, I employ the grid of upper atmosphere models presented in Kubyshkina & Fossati (2021). This grid is based on the hydrodynamic 1D model by Kubyshkina et al. (2018) described in brief at the beginning of section 3 and includes ~ 10000 model planets with masses of 1–108.6 $M_\oplus$ and radii of 1–10 $R_\oplus$ orbiting stars with masses between 0.4 $M_\odot$ and 1.3 $M_\odot$. The orbital distances for each stellar mass cover the range of equilibrium temperatures of 300–2000 K, and the irradiation levels at all orbits vary between the values typical for young stars (near the time of protoplanetary disk dispersal) and for stars at the end of the main sequence (~ 10 Gyr). By construction, the grid is dominated by close-in planets and, further, the non-physical model planets and those where the hydrodynamic approach is not applicable were excluded from consideration. In particular, this includes planets with mean densities lower than 0.03 g/cm^3 or higher than that expected for the rocky core of the given mass, and planets with exobases below the sonic level. The consideration in Kubyshkina & Fossati (2021) also excludes the planets with Roche radii smaller than 1.5 $R_{\rm pl}$. In the present work, however, I include them for completeness.

In the top panel of Figure 5, I show the atmospheric mass loss rates of the grid planets against the generalized Jeans escape parameter $\Lambda = (GM_{\rm pl}m_{\rm H})/(k_{\rm b}T_{\rm eq}R_{\rm pl})$ (the same as parameter $\lambda_{\rm ex}$ in section 2.1, but calculated at the photosphere). To distinguish between the different cases of hydrodynamic outflow, I use the following formalisation. First, to separate the model planets, where the input from the own thermal energy is more significant than the XUV heating, I compare the mass loss rates predicted by hydrodynamic modeling with the ones predicted by energy-limited approximation (Erkaev et al. 2007), assuming that the atmospheric escape is purely driven by stellar XUV

$$\dot{M}_{\rm EL} = \pi \frac{\eta \Phi_{\rm XUV} R_{\rm eff}^2 R_{\rm pl}}{G M_{\rm pl}}. \tag{3.9}$$

Here, $\Phi_{\rm XUV}$ is the XUV flux received by the planets, and the heating efficiency coefficient η is taken 0.15 to consist with the hydrodynamic models. $R_{\rm eff}$ is an effective radius of the XUV absorption, reflecting the narrow interval where the high energy irradiation from the host star is absorbed in the planetary atmosphere (see the discussion in section 3.1), reduced to one specific distance. Taking $R_{\rm eff} = R_{\rm pl}$, as is done in the numerous studies, leads in general to a drastic underestimation of the atmospheric mass loss rates. Adopting $R_{\rm eff}$ defined in the hydrodynamic simulations, in turn, would make the predicted mass-loss rates closer to those in the grid but would make the comparison between the two predictions less meaningful. The effective radii for planets with outflows driven mainly by their own thermal energy, as the one discussed in section 3.2, are formally set at the upper boundary of the simulation domain (see Kubyshkina et al. 2018, for the detail). Thus, the estimates obtained with Equation 3.9 would increase but become physically meaningless. Therefore, to define $R_{\rm eff}$ I adopt here the analytical equation (Chen & Rogers 2016)

$$R_{\rm eff} = R_{\rm pl} + H \ln\left(\frac{P_{\rm photo}}{P_{\rm XUV}}\right), \tag{3.10}$$

where H is the atmospheric scale height, $P_{\rm photo}$ is the pressure at the photosphere, and $P_{\rm XUV}$ is the pressure at the XUV absorption level approximated as $(GM_{\rm pl}m_{\rm H})/(\sigma_{\rm 20eV}R_{\rm pl}^2)$. In the latter, $\sigma_{\rm 20eV}$ is the absorption cross-section of hydrogen for a photon energy of 20 eV. Equation 3.10 predicts the effective radii of the XUV absorption similar to those obtained from the hydrodynamic models for planets with the outflow predominantly driven by the stellar XUV heating. Including it in Equation 3.9, therefore, leads to the estimation of the atmospheric mass loss rates comparable to the estimates from the hydrodynamic models for the XUV-driven escape (gray dots in Figure 5). Thus, to distinguish the planets where the winds are mainly driven by their own thermal energy

https://doi.org/10.1017/S1743921322004598 Published online by Cambridge University Press

(not accounted for in the Equation 3.9) and the input from the stellar XUV becomes minor, I filter the model planets with atmospheric mass loss rates $\dot{M}$ larger than 10 times the mass loss rates predicted by energy-limited approximation $\dot{M}_{\rm EL}$ (orange dots in Figure 5). Some of these planets can be further affected by the tidal forces, and to avoid mixing up the two effects, I further exclude from this group the planets with the Roche radii smaller than $2R_{\rm pl}$. Additionally, I highlight in Figure 5 the planets in "transitional" state given by the conditions $\dot{M} = 5 - 10 \times \dot{M}_{\rm EL}$ and $R_{\rm roche} > R_{\rm pl}$ (cyan dots).

The Roche radius of the planet is the point on the star-planet line, where the gravitation forces of the planet and the star are balanced. Therefore, its position relative to the photosphere radius is a good proxy of the degree to which the tidal forces of the host star affect the atmospheric outflow. For grid planets, the tidal effects become significant when the Roche lobe is smaller than about $2R_{\rm pl}$ (violet points in Figure 5), and, similarly to the case considered in section 3.3, become dominant when the Roche lobe lies below $\sim 1.5R_{\rm pl}$ (green points in Figure 5). One can see, that the violet points in Figure 5 ($R_{\rm roche} = 1.5 - 2 \times R_{\rm pl}$) represent a transitional state between the tidally driven outflow and planetary winds driven by the internal thermal energy of planets (for $\Lambda \lesssim 20$) or the XUV-driven planetary winds ($\Lambda > 20$).

Speaking about the parameters of planets in the different groups, the group planets with the outflow driven by their own thermal energy should be dominated by planets with low gravity and high temperature, as, in this case, the relation of the gravitational energy to the thermal energy (given, in essence, by the parameter Λ) is small. Indeed, most of the group of orange points in Figure 5 is concentrated at $\Lambda < 20$. The occurrence rate of different equilibrium temperatures of planets in this group is strongly biased by the construction of the grid, so in Figure 5 I only demonstrate the distribution of planets in this group across planetary masses (bottom left panel). One can see, that the majority of planets in this group have masses below $10\,M_{\oplus}$, and their fraction in the total number of grid planets with $R_{\rm roche} > 2R_{\rm pl}$ (shown by the empty bins) is consistently increasing with decreasing mass. However, the number of such planets remains significant up to 20–$30\,M_{\oplus}$ and some single planets are present up to $50\,M_{\oplus}$. The shape of the distribution for all grid planets with $R_{\rm roche} > 2R_{\rm pl}$ is mainly defined by the density cut described at the beginning of this section.

Formally, the potential number of planets whose outflow is dominated by tidal effects increases with decreasing stellar mass, as is shown by the empty histogram bins in the bottom right panel of Figure 5. To plot these bins, I calculated the Roche lobes for all the planets in the grid parameter space, applied the density filter described above, and filtered the planets with $R_{\rm roche} < 1.5R_{\rm pl}$. However, a significant fraction of these planets have the Roche lobes that lie below the photosphere level – and this fraction also increases towards lower stellar masses. Therefore, the actual number of "tidally dominated" planets existing in the grid (which, in fact, only includes planets with $R_{\rm roche} > 1.2R_{\rm pl}$) maximizes at the stellar mass of $0.6\,M_{\odot}$.

4. Magnetic field and the escape of planetary atmospheres

The effect of a magnetic field, if present at the planet, is essential in describing escaping atmospheres and their interaction with magnetized stellar winds, and therefore, in the interpretation of the observations (see, e.g., Matsakos et al. 2015; Villarreal D'Angelo et al. 2018; Carolan et al. 2021; Cohen et al. 2022). However, the effect of the magnetic field on planetary winds, and specifically on atmospheric mass loss rates, can be ambiguous. While for compact atmospheres and strong enough fields, the upper atmosphere does not interact with the stellar wind directly anymore, reducing the effects of erosion and ion pick-up, some processes discussed in Section 2.3 can lead to additional heating or intensification of ion escape in specific regions. Thus, at

https://doi.org/10.1017/S1743921322004598 Published online by Cambridge University Press

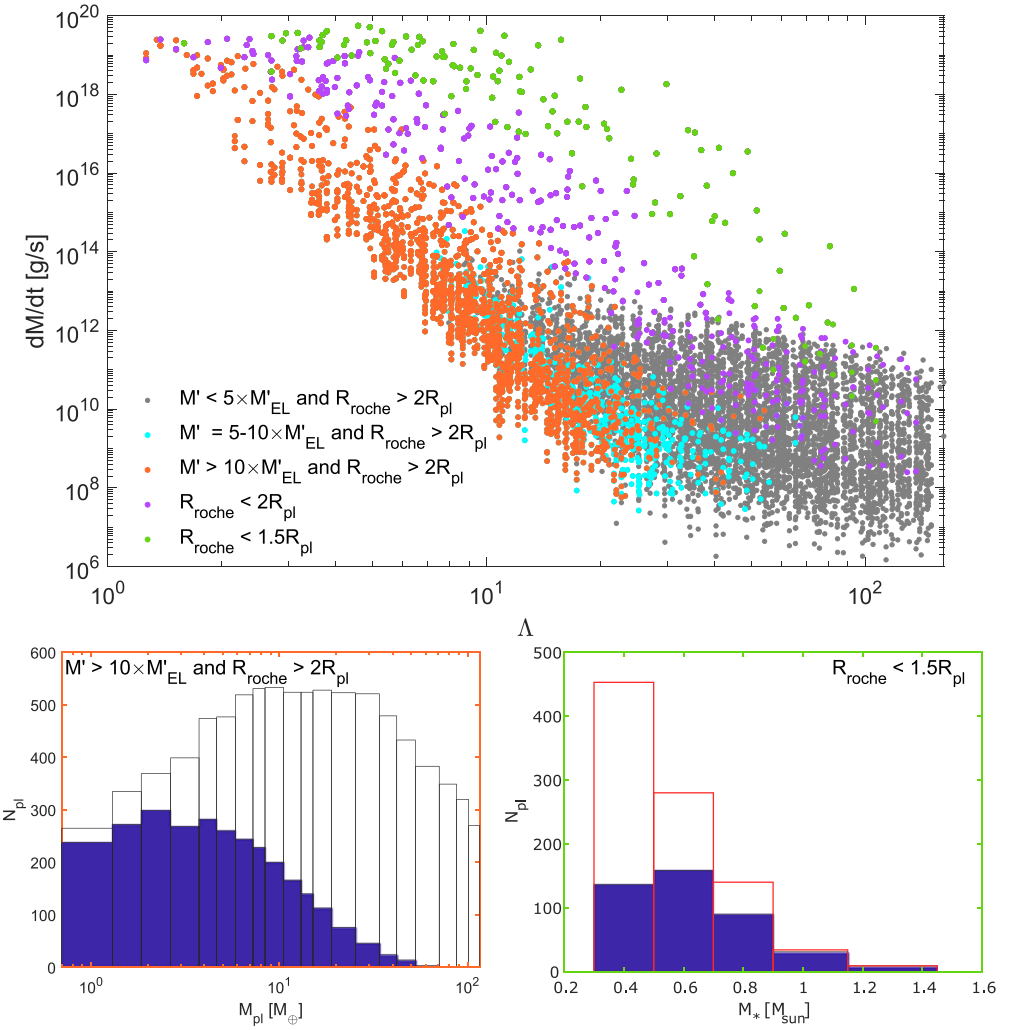

Figure 5. Top panel: atmospheric mass loss rates against the gravitational Jeans parameter calculated at the photosphere. Color code reflects the presumable major driver of the atmospheric escape. Gray points represent XUV-dominated planets, orange points highlight the planets with dominating internal thermal energy, and green points show the planets dominated by tidal effects. Cyan and violet points correspond to the transitional regimes. See the detailed discussion in the text. Bottom left panel: number of planets in different planetary mass bins in the grid of upper atmosphere models. The empty bins show the total number of planets in the grid with $R_{\rm roche} > 2R_{\rm pl}$, and the blue bins correspond to the planets with atmospheric mass loss dominated by their own thermal energy of the planet. Bottom right panel: number of planets with Roche radius below 1.5 of the photosphere radius. The empty bins show the total number of such planets within the parameter space of the grid and the blue bins reflect the actual number of planets in the grid. Note, that a significant fraction of planets shown by the empty bins were in general not considered, as the Roche lobe lies below the photosphere level. All plots are based on the grid of upper atmosphere models presented in Kubyshkina & Fossati (2021).

strongly magnetized planets, polar outflow can represent one of the major escape sources both in the context of hydrodynamic (e.g., Carolan et al. 2021) and non-thermal (e.g., Zhang et al. 2022) escape.

For terrestrial planets in Solar System (dominated by non-thermal escape processes), it was shown that a weak magnetic field can intensify the escape, while the strong field

https://doi.org/10.1017/S1743921322004598 Published online by Cambridge University Press

is, in general, expected to be protective (Gunell et al. 2018; Sakai et al. 2018; Egan et al. 2019; Ramstad & Barabash 2021). Further on, for the crustal magnetic field at Mars, the overall effect on the atmospheric mass loss depends on the configuration and inclination angle of the magnetic field (Weber et al. 2021; Li et al. 2022; Curry et al. 2022).

For Hot Jupiters, where planetary winds are driven by hydrodynamic processes, models predict significant suppression of the atmospheric mass losses for magnetic field strength above 0.1–3 G (see Owen & Adams 2014; Trammell et al. 2014; Khodachenko et al. 2015; Arakcheev et al. 2017; Khodachenko et al. 2021). For more moderate planets hosting hydrogen-dominated atmospheres, the effect remains unclear. E.g., Carolan et al. (2021) predict for 0.7 $M_{\rm jup}$ planet a small increase in escape for magnetic field strength increasing from 0 to 5 G.

To summarize, the actual effect of magnetic fields on planetary winds depends on the type of planetary atmospheres, parameters and position of the planet, and configuration of the field itself.

5. Conclusions

The processes driving planetary winds are extremely various, and spread from microphysical kinetic processes to global hydrodynamic flows. Relevant mechanisms vary in dependence on the properties of the planet, its orbit, type of the atmosphere, and the age and mass of the host star. Thus, escape from evolved terrestrial-like planets near the habitable zone is, in general, dominated by non-thermal escape processes, including ion escape and the interaction with stellar winds. However, at young ages, when the stellar flux is high even at relatively far orbits, the planetary wind is expected to be driven by thermal processes. If such escape is hydrodynamic or kinetic (Jeans escape) is defined by the parameters of a planet and the energy budget of its atmosphere.

Planetary winds from Neptune-like to Jupiter-like planets are, in general, hydrodynamic. Their atmospheric mass loss rates dominate, typically, over those of kinetic processes and spread over a few orders of magnitude depending on planetary and stellar parameters. The mass loss rates maximize for low-gravity hot planets, where the outflow is driven by their own thermal energy rather than stellar irradiation. For the majority of planets, however, the hydrodynamic outflow is driven by stellar XUV radiation. The mass loss rates, in this case, span between 10^7–10^{12} g/s. Finally, for close-in planets, the tidal forces of the host star can play a significant role. Their influence increases for planets orbiting low-mass stars due to closer orbital distances.

Given the wide range of possible driving mechanisms, modeling planetary winds represents a non-trivial task, specifically for planets outside of Solar System. Even though some mechanisms depend mainly on general parameters of the planet, such as its mass, radius, and temperature (which are, to some extent, measurable), in general case one has to deal with parameters that can be poorly constrained. In particular, the content of exoplanetary atmospheres, crucial for non-thermal processes is typically unknown; therefore, modeling these processes should, in the best case, include the analysis of specific atmospheres for stability in the evolutionary context. The latter is, however, further complicated by the uncertain evolution history of the host star (Kubyshkina et al. 2019). The same problem holds for magnetic fields at exoplanets, which cannot, to date, be directly measured. Therefore, the presence of magnetic fields can potentially only be constrained by the effect it causes on planetary outflow and its interaction with stellar wind and, hence, on observations (e.g., Lyα). However, given the wide range of parameters affecting these processes, the task appears difficult for most of the planets.

Besides the intrinsic parameters of the planet, its environment plays a crucial role. It includes, in the first place, the parameters of the host star and the orbital distance of the planet. In general, the latter can be constrained from the observations with good

https://doi.org/10.1017/S1743921322004598 Published online by Cambridge University Press

accuracy, while some of the stellar parameters remain unknown and are set on the basis of theoretical and empirical models. This includes, in particular, stellar EUV radiation and parameters of stellar winds (see, e.g., Vidotto 2021).

References

Allan, A. & Vidotto, A. A. 2019, MNRAS, 490, 3760. doi:10.1093/mnras/stz2842

Arakcheev, A. S., Zhilkin, A. G., Kaigorodov, P. V., et al. 2017, Astronomy Reports, 61, 932. doi:10.1134/S1063772917110014

Arras,, P. & Socrates, A. 2010, ApJ, 714, 1. doi:10.1088/0004-637X/714/1/1

Batygin, K. & Stevenson, D. J. 2010, ApJ Letters, 714, L238. doi:10.1088/2041-8205/714/2/L238

Bodenheimer, P., Lin, D. N. C., & Mardling, R. A. 2001, ApJ, 548, 466. doi:10.1086/318667

Caldiroli, A., Haardt, F., Gallo, E., et al. 2021, A&A, 655, A30. doi:10.1051/0004-6361/202141497

Caldiroli, A., Haardt, F., Gallo, E., et al. 2022, A&A, 663, A122. doi:10.1051/0004-6361/202142763

Carolan, S., Vidotto, A. A., Hazra, G., et al. 2021, MNRAS, 508, 6001. doi:10.1093/mnras/stab2947

Carolan, S., Vidotto, A. A., Plavchan, P., et al. 2020, MNRAS, 498, L53. doi:10.1093/mnrasl/slaa127

Cecchi-Pestellini, C., Ciaravella, A., Micela, G., et al. 2009, A&A, 496, 863. doi:10.1051/0004-6361/200809955

Chamberlain, J. W. 1963, Planetary and Space Science, 11, 901. doi:10.1016/0032-0633(63)90122-3

Chamberlain, J. W. 1969, ApJ, 155, 711. doi:10.1086/149905

Chen, H. & Rogers, L. A. 2016, ApJ, 831, 180. doi:10.3847/0004-637X/831/2/180

Christie, D., Arras, P., & Li, Z.-Y. 2016, ApJ, 820, 3. doi:10.3847/0004-637X/820/1/3

Cohen, O., Alvarado-Gómez, J. D., Drake, J. J., et al. 2022, ApJ, 934, 189. doi:10.3847/1538-4357/ac78e4

Cubillos, P., Erkaev, N. V., Juvan, I., et al. 2017, MNRAS, 466, 1868. doi:10.1093/mnras/stw3103

Curry, S. M., Tatum, P., Mitchell, D., et al. 2022, MNRAS, 517, L121. doi:10.1093/mnrasl/slac099

Dalgarno, A., Yan, M., & Liu, W. 1999, ApJS, 125, 237. doi:10.1086/313267

Dayhoff, M. O., Eck, R. V., Lippincott, E. R., et al. 1967, Science, 155, 556. doi:10.1126/science.155.3762.556

Egan, H., Jarvinen, R., Ma, Y., et al. 2019, MNRAS, 488, 2108. doi:10.1093/mnras/stz1819

Erkaev, N. V., Kulikov, Y. N., Lammer, H., et al. 2007, A&A, 472, 329. doi:10.1051/0004-6361:20066929

Erkaev, N. V., Lammer, H., Odert, P., et al. 2015, MNRAS, 448, 1916. doi:10.1093/mnras/stv130

Erkaev, N. V., Lammer, H., Odert, P., et al. 2016, MNRAS, 460, 1300. doi:10.1093/mnras/stw935

Erkaev, N., Scherf, M., Herbort, O., et al. 2022, arXiv:2209.14691 (accepted for publication in MNRAS)

Fortney, J. J., Dawson, R. I., & Komacek, T. D. 2021, Journal of Geophysical Research (Planets), 126, e06629. doi:10.1029/2020JE006629

Fulton, B. J., Petigura, E. A., Howard, A. W., et al. 2017, AJ, 154, 109. doi:10.3847/1538-3881/aa80eb

Fulton, B. J. & Petigura, E. A. 2018, AJ, 156, 264. doi:10.3847/1538-3881/aae828

Ginzburg, S., Schlichting, H. E., & Sari, R. 2016, ApJ, 825, 29. doi:10.3847/0004-637X/825/1/29

Ginzburg, S. & Sari, R. 2016, ApJ, 819, 116. doi:10.3847/0004-637X/819/2/116

Ginzburg, S., Schlichting, H. E., & Sari, R. 2018, MNRAS, 476, 759. doi:10.1093/mnras/sty290

Gronoff, G., Arras, P., Baraka, S., et al. 2020, Journal of Geophysical Research (Space Physics), 125, e27639. doi:10.1029/2019JA027639

Gross, S. H. 1972, Journal of Atmospheric Sciences, 29, 214. doi:10.1175/1520-0469(1972)029<0214:OTETOH>2.0.CO;2
Gunell, H., Maggiolo, R., Nilsson, H., et al. 2018, A&A, 614, L3. doi:10.1051/0004-6361/201832934
Gupta, A. & Schlichting, H. E. 2019, MNRAS, 487, 24. doi:10.1093/mnras/stz1230
Hazra, G., Vidotto, A. A., Carolan, S., et al. 2022, MNRAS, 509, 5858. doi:10.1093/mnras/stab3271
Hunten, D. M. 1973, Journal of Atmospheric Sciences, 30, 1481. doi:10.1175/1520-0469(1973)030<1481:TEOLGF>2.0.CO;2
Hunten, D. M. 1982, Planetary and Space Science, 30, 773. doi:10.1016/0032-0633(82)90110-6
Hunten, D. M., Pepin, R. O., & Walker, J. C. G. 1987, Icarus, 69, 532. doi:10.1016/0019-1035(87)90022-4
Johnson, R. E. 1994, SSR, 69, 215. doi:10.1007/BF02101697
Johnson, R. E., Combi, M. R., Fox, J. L., et al. 2008, SSR, 139, 355. doi:10.1007/s11214-008-9415-3
Khodachenko, M. L., Shaikhislamov, I. F., Lammer, H., et al. 2015, ApJ, 813, 50. doi:10.1088/0004-637X/813/1/50
Khodachenko, M. L., Shaikhislamov, I. F., Lammer, H., et al. 2021, MNRAS, 507, 3626. doi:10.1093/mnras/stab2366
King, G. W. & Wheatley, P. J. 2021, MNRAS, 501, L28. doi:10.1093/mnrasl/slaa186
Kislyakova, K. G., Lammer, H., Holmström, M., et al. 2013, Astrobiology, 13, 1030. doi:10.1089/ast.2012.0958
Kislyakova, K. G., Fossati, L., Johnstone, C. P., et al. 2018, ApJ, 858, 105. doi:10.3847/1538-4357/aabae4
Koskinen, T. T., Lavvas, P., Huang, C., et al. 2022, ApJ, 929, 52. doi:10.3847/1538-4357/ac4f45
Kubyshkina, D., Fossati, L., Erkaev, N. V., et al. 2018, A&A, 619, A151. doi:10.1051/0004-6361/201833737
Kubyshkina, D., Cubillos, P. E., Fossati, L., et al. 2019, ApJ, 879, 26. doi:10.3847/1538-4357/ab1e42
Kubyshkina, D., Vidotto, A. A., Fossati, L., et al. 2020, MNRAS, 499, 77. doi:10.1093/mnras/staa2815
Kubyshkina, D. I. & Fossati, L. 2021, Research Notes of the American Astronomical Society, 5, 74. doi:10.3847/2515-5172/abf498
Kubyshkina, D., Vidotto, A. A., Villarreal D'Angelo, C., et al. 2022, MNRAS, 510, 2111. doi:10.1093/mnras/stab3594
Kulikov, Y. N., Lammer, H., Lichtenegger, H. I. M., et al. 2007, SSR, 129, 207. doi:10.1007/s11214-007-9192-4
Lammer, H., Selsis, F., Ribas, I., et al. 2003, ApJ Letters, 598, L121. doi:10.1086/380815
Lammer, H., Kasting, J. F., Chassefière, E., et al. 2008, SSR, 139, 399. doi:10.1007/s11214-008-9413-5
Lammer, H., Leitzinger, M., Scherf, M., et al. 2020, Icarus, 339, 113551. doi:10.1016/j.icarus.2019.113551
Lammer, H., Scherf, M., Kurokawa, H., et al. 2020, SSR, 216, 74. doi:10.1007/s11214-020-00701-x
Lecavelier des Etangs, A., Vidal-Madjar, A., McConnell, J. C., et al. 2004, A&A, 418, L1. doi:10.1051/0004-6361:20040106
Lee, Y., Combi, M. R., Tenishev, V., et al. 2015, GRL, 42, 9015. doi:10.1002/2015GL065291
Li, S., Lu, H., Cao, J., et al. 2022, ApJ, 931, 30. doi:10.3847/1538-4357/ac6510
Lopez, E. D., Fortney, J. J., & Miller, N. 2012, ApJ, 761, 59. doi:10.1088/0004-637X/761/1/59
Matsakos, T., Uribe, A., & Königl, A. 2015, A&A, 578, A6. doi:10.1051/0004-6361/201425593
Mihalas, D. & Mihalas, B. W. 1984, New York, Oxford University Press, 1984, 731 p.
Mordasini, C. 2020, A&A, 638, A52. doi:10.1051/0004-6361/201935541
Murray-Clay, R. A., Chiang, E. I., & Murray, N. 2009, ApJ, 693, 23. doi:10.1088/0004-637X/693/1/23

Odert, P., Lammer, H., Erkaev, N. V., et al. 2018, Icarus, 307, 327. doi:10.1016/j.icarus.2017.10.031
Owen, J. E. & Jackson, A. P. 2012, MNRAS, 425, 2931. doi:10.1111/j.1365-2966.2012.21481.x
Owen, J. E. & Adams, F. C. 2014, MNRAS, 444, 3761. doi:10.1093/mnras/stu1684
Owen, J. E. & Wu, Y. 2017, ApJ, 847, 29. doi:10.3847/1538-4357/aa890a
Öpik, E. J. 1963, Geophysical Journal, 7, 490. doi:10.1111/j.1365-246X.1963.tb07091.x
Pepin, R. O. 1991, Icarus, 92, 2. doi:10.1016/0019-1035(91)90036-S
Ramstad, R. & Barabash, S. 2021, SSR, 217, 36. doi:10.1007/s11214-021-00791-1
Sakai, S., Seki, K., Terada, N., et al. 2018, GRL, 45, 9336. doi:10.1029/2018GL079972
Salz, M., Schneider, P. C., Czesla, S., et al. 2015, A&A, 576, A42. doi:10.1051/0004-6361/201425243
Salz, M., Schneider, P. C., Czesla, S., et al. 2016, A&A, 585, L2. doi:10.1051/0004-6361/201527042
Salz, M., Czesla, S., Schneider, P. C., et al. 2016, A&A, 586, A75. doi:10.1051/0004-6361/201526109
Sekiya, M., Nakazawa, K., & Hayashi, C. 1980, Progress of Theoretical Physics, 64, 1968. doi:10.1143/PTP.64.1968
Shematovich, V. I., Bisikalo, D. V., & Gerard, J. C. 1994, JGR, 99, 23217. doi:10.1029/94JA01769
Shematovich, V. I., Ionov, D. E., & Lammer, H. 2014, A&A, 571, A94. doi:10.1051/0004-6361/201423573
Shizgal, B. & Lindenfeld, M. J. 1982, JGR, 87, 853. doi:10.1029/JA087iA02p00853
Shizgal, B. & Blackmore, R. 1986, Planetary and Space Science, 34, 279. doi:10.1016/0032-0633(86)90133-9
Shizgal, B. D. & Arkos, G. G. 1996, Reviews of Geophysics, 34, 483. doi:10.1029/96RG02213
Trammell, G. B., Li, Z.-Y., & Arras, P. 2014, ApJ, 788, 161. doi:10.1088/0004-637X/788/2/161
Vidal-Madjar, A. 1978, GRL, 5, 29. doi:10.1029/GL005i001p00029
Vidotto, A. A., Fares, R., Jardine, M., et al. 2015, MNRAS, 449, 4117. doi:10.1093/mnras/stv618
Vidotto, A. A. & Cleary, A. 2020, MNRAS, 494, 2417. doi:10.1093/mnras/staa852
Vidotto, A. A. 2021, Living Reviews in Solar Physics, 18, 3. doi:10.1007/s41116-021-00029-w
Villarreal D'Angelo, C., Esquivel, A., Schneiter, M., et al. 2018, MNRAS, 479, 3115. doi:10.1093/mnras/sty1544
Volkov, A. N., Johnson, R. E., Tucker, O. J., et al. 2011, ApJ Letters, 729, L24. doi:10.1088/2041-8205/729/2/L24
Watson, A. J., Donahue, T. M., & Walker, J. C. G. 1981, Icarus, 48, 150. doi:10.1016/0019-1035(81)90101-9
Weber, T., Brain, D., Xu, S., et al. 2021, Journal of Geophysical Research (Space Physics), 126, e29234. doi:10.1029/2021JA029234
Wu, Y. & Lithwick, Y. 2013, ApJ, 763, 13. doi:10.1088/0004-637X/763/1/13
Yelle, R. V. 2004, Icarus, 170, 167. doi:10.1016/j.icarus.2004.02.008
Zahnle, K. J. & Kasting, J. F. 1986, Icarus, 68, 462. doi:10.1016/0019-1035(86)90051-5
Zhang, H., Fu, S., Fu, S., et al. 2022, ApJ, 937, 4. doi:10.3847/1538-4357/ac8a93